HHS Public Access

Author manuscript

Opt Mater (Amst). Author manuscript; available in PMC 2019 December 23.

Published in final edited form as:

Opt Mater (Amst). 2018 October ; 84: 345–353. doi:10.1016/j.optmat.2018.07.031.

Photostable and efficient upconverting nanocrystal-based chemical sensors

Cheryl A. Tajon, **Hao Yang**, **Bining Tian**, **Yue Tian**, **Peter Ercius**, **P. James Schuck**[†], **Emory M. Chan**, **Bruce E. Cohen**

The Molecular Foundry, Lawrence Berkeley National Laboratory, Berkeley, California 94720 USA

Abstract

Chemical sensing in living systems demands optical sensors that are bright, stable, and sensitive to the rapid dynamics of chemical signaling. Lanthanide-doped upconverting nanoparticles (UCNPs) efficiently convert near infrared (NIR) light to higher energy emission and allow biological systems to be imaged with no measurable background or photobleaching, and with reduced scatter for subsurface experiments. Despite their advantages as imaging probes, UCNPs have little innate chemical sensing ability and require pairing with organic fluorophores to act as biosensors, although the design of stable UCNP-fluorophore hybrids with efficient upconverted energy transfer (UET) has remained a challenge. Here, we report Yb^{3+}- and Er^{3+}-doped UCNP-fluorophore conjugates with UET efficiencies up to 88%, and photostabilities 100-fold greater by UET excitation than those of the free fluorophores under direct excitation. Despite adding distance between Er^{3+} donors and organic acceptors, thin inert shells significantly enhance overall emission without compromising UET efficiency. This can be explained by the large increase in quantum yield of Er^{3+} donors at the core/shell interface and the large number of fluorophore acceptors at the surface. Sensors excited by UET show increases in photostability well beyond those reported for other methods for increasing the longevity of organic fluorophores, and those covalently attached to UCNP surface polymers show greater chemical stability than those directly coordinated to the nanocrystal surface. By conjugating other fluorescent chemosensors to UCNPs, these hybrids may be extended to a series of NIR-responsive biosensors for quantifying the dynamic chemical populations critical for cell signaling.

Keywords

Upconverting nanoparticles; Sensors; Fluorescence; Energy transfer; Photostability

1. Introduction

Our understanding of chemical signaling in living systems has arisen largely from fluorescent chemical sensors able to detect dynamic populations of metal ions, metabolites, secondary messengers, and complex biomolecules within functional cells.[1–2] Starting with probes of Ca^{2+} ions,[3] an expansive suite of organic fluorophores and genetically encoded

becohen@lbl.gov.

[†]*Present Address:* Department of Mechanical Engineering, Columbia University, New York, NY 10027 USA

proteins has been engineered for chemical sensing of diverse targets with the selectivity, dynamic range, stability, and brightness necessary for imaging complex living systems. The extension of these optical biosensors from simple cell culture systems to intact tissue adds the challenge of excitation and emission through tissue that scatters, absorbs, and fluoresces. Each of these optical processes is dependent on the wavelength of light being used: most biomolecules absorb or emit ultraviolet (UV) or visible light, while scattering decreases significantly at longer wavelengths in the near infrared (NIR).[4–5] Although the NIR contains tissue-transparent windows that might be exploited for the development of optical biosensors, most useful chemical sensing probes are excited by UV or visible light.[1–3, 6]

Lanthanide-doped upconverting nanoparticles (UCNPs) absorb multiple NIR photons and emit at higher energies with efficiencies orders of magnitude higher than those of the best 2-photon fluorophores.[7–8] UCNPs can be imaged in the absence of cellular autofluorescence or measurable photobleaching, even under prolonged single-particle excitation.[9–10] UCNPs make use of energy transfer upconversion between $4f^N$ electronic states of neighboring lanthanide (Ln^{3+}) ions, in which sensitizer ions sequentially transfer absorbed energy to luminescent emitter ions, both of which are doped into a low-phonon nanocrystal host matrix. For many applications, β-phase $NaYF_4$ nanocrystals doped with 20% Yb^{3+} sensitizer and a low percentage of Er^{3+} or Tm^{3+} emitter are most efficient and can be excited with modest continuous wave (CW) lasers. Addition of inert epitaxial shells to these UCNPs has been shown to significantly enhance emission by reducing Yb^{3+}-mediated energy migration to high-vibrational-frequency modes of surface oleate ligands or solvent.[7, 11–16]

While UCNPs are inherently sensitive to temperature[17–18] and mechanical force,[19] they have little innate chemical sensing ability and require pairing with external probes to act as biosensors. A series of ions, toxins, and biomolecular interactions have been imaged using UCNPs coupled with organic sensors, with organic small molecules typically quenching one or more Er^{3+} luminescence bands, enabling ratiometric imaging.[20–25] UCNP complexes with organic fluorophores[26–30] and fluorescent proteins[31] have also been reported, but upconverted energy transfer (UET) in these systems is less well understood or optimized. Efficiency for UET, defined here as resonant energy transfer from UCNP Ln^{3+} donors to energy acceptors, varies wildly depending on specifics of UCNP composition and how the UCNP-fluorophore hybrids are constructed[20, 26–27, 30] [32][32][32][32][32][32] Here, we report chemically stable UCNP-fluorophore complexes with almost 90% UET efficiency and up to 100-fold increase in photostability compared to direct fluorophore excitation. We have characterized UET as a function of nanocrystal composition and structure, fluorophore:UCNP stoichiometry, attachment method, and excitation laser power. We find that 88% UET can be achieved with core/shell UCNPs at confocal laser powers, which can be explained by the large increase in quantum yield of Er^{3+} donors at the core/shell interfaces and the large number of fluorophore acceptors at the surface. Thin, inert $NaYF_4$ shells improve overall brightness >1000-fold without decreasing UET efficiency,[33] despite adding 2 nm distance between Er^{3+} donor and organic acceptor. Sensors excited by UET show increases in photostability well beyond those reported for other methods for increasing the longevity of organic fluorophores, and those covalently attached to UCNP surface polymers show significantly greater chemical stability than those directly coordinated to the

nanocrystal surface. These findings can be applied as general design principles for the synthesis of bright, stable UCNP-based fluorescent sensors for imaging a variety of analytes in living systems.

2. Experimental Section

2.1 Synthesis of 8-nm β -$NaYF_4$: 20% Yb, x% Er, 20% Gd nanocrystals

β-Phase UCNPs were synthesized as described,[34] with minor modifications, with Er^{3+} content from 2 to 60%. To synthesize $NaYF_4$: 20% Yb, 20% Er, 20% Gd nanocrystals: $YbCl_3 \cdot H_2O$ (0.080 mmol, 32 mg, Strem), YCl_3 (0.16 mmol, 31 mg), $ErCl_3$ (0.08 mmol, 22 mg), $GdCl_3$ (0.080 mmol, 21 mg), oleic acid (3.25 g), and 1-octadecene (ODE, 4 mL) were stirred in a flask with an in-reaction thermocouple and were heated at 110 °C under vacuum, and purged with N_2 every 15 min. After 1 h, the dissolved lanthanides were cooled under N_2, and sodium oleate (1.25 mmol, 382 mg), NH_4F (2.0 mmol, 74 mg), and ODE (3 mL) were added to the flask. The reaction mixture was stirred under vacuum at room temperature for 30 min and then heated at 315 °C for 45 min. The reaction flask was cooled with a strong stream of air until the thermocouple read 40 °C. The product was transferred to a 50-mL centrifuge tube, 10 mL of EtOH added, and the tube centrifuged at 3000 × *g* for 3 min. The supernatant was decanted and 3 mL of hexane used to wash the reaction flask was added to the pellet, which was sonicated to ensure it was well-dispersed. The tube was centrifuged at 3000 × *g* for 3 min and the supernatant transferred to a new tube, leaving behind NaF impurities. To the dispersed UCNPs, 5 mL of EtOH was added and the tube centrifuged again at 3000 × *g* for 3 min. The pellet was dispersed in 1 mL of hexane, washed with 5 mL of EtOH two additional times, and the resulting pellet was dispersed in 15 mL of anhydrous hexane.

2.2 Synthesis of core/shell UCNPs

β -$NaYF_4$: 20% Gd shells were grown on β-$NaYF_4$: 20% Yb, x% Er, 20% Gd UCNPs with a layer-by-layer protocol,[35] using 28 nmol of core UCNPs. For 2-nm shell growth on 8-nm β-$NaYF_4$: 20% Yb, 20% Er, 20% Gd UCNPs, a hexane dispersion of core UCNPs was added to a 3-neck, 50-mL flask and the hexane evaporated under N_2. Oleic acid (4 mL) and ODE (6 mL) were added and the flask stirred at 70 °C for 1 hour under vacuum. In separate flasks, Ln oleates were prepared by heating YCl_3 (0.40 mmol, 78 mg), $GdCl_3$ (0.10 mmol, 26 mg), oleic acid (2 mL), and 1-octadecene (3 mL) at 110 °C for 1 h under vacuum; and sodium trifluoroacetate (1.20 mmol, 16 mg) was dissolved in oleic acid (3 mL) and stirred at room temperature for 1 hour under vacuum. The UCNPs flask was purged with N_2 and heated at 280 °C for 10 min, allowing the temperature to stabilize. Shell precursors were injected as in Table S2, with sequential injections of lanthanide and Na/F precursors performed every 15 min. After four rounds of injections, the reaction was allowed to stir for an additional 30 min at 280 °C, and a strong stream of air to the flask was used for cooling. Core/shell UCNPs were isolated and stored using the same protocol for core UCNPs.

2.3 Synthesis of POA amphiphilic copolymer

To a round-bottom flask was added 800 mg of polyacrylic acid (M_W ~ 2000, Sigma Aldrich, 0.40 mmol), 1.40 g of *N*-hydroxysuccinimide (12 mmol), 60 mL of 200 mM HEPES buffer

(pH 7.5), and 20 mL of EtOH. In separate 50 mL tubes, 1.90 mL of *tert*-butyl *N*-(2-aminoethyl)carbamate (12.0 mmol) and 992 μL of 1-octylamine (6.0 mmol) were each dissolved in 20 mL of EtOH. Both amine solutions of amine were added to the reaction and the pH adjusted to pH 7.5 using 5 M NaOH. EDC (22.0 mmol, 3.40 g) was added in 3 parts over 18 h, with the pH readjusted to 7.5 before the final addition. The resulting product was distributed equally among four 50 mL tubes and each concentrated to 5 mL under N_2. The tubes were centrifuged at 5000 × *g* for 10 min at 4 °C, the supernatant decanted, and 20 mL of H_2O was added to each tube. The tubes were sonicated for 15 min and then centrifuged at 5000 × *g* for 10 min at 4 °C. Supernatants were decanted and each pellet was dissolved in 5 mL of trifluoroacetic acid, which was then evaporated overnight under a stream of N_2. The resulting oil was dissolved in 20 mL of 30% EtOH and the pH raised to 5 with concentrated NH_4OH. The solution was distributed equally among two dialysis cassettes (3500 Da MWCO, Thermo Fisher) and dialyzed against 3 × 4 L of H_2O, causing the polymer to precipitate. The polymer was removed from the cassettes with EtOH and concentrated under N_2 to remove all EtOH. The product, poly(*n*-octylacrylamide)-*co*-poly(2-aminoethylacrylamide) random amphiphilic copolymer (POA) with a 2:1 amine:C_8 ratio, was lyophilized to a white powder 1.30 g (~90% yield).

2.4 UCNP polymer encapsulation

Following similar encapsulation procedures for quantum dots with amphiphilc polymers, [36] the UCNP-polymer stoichiometries were 1:2900 for core UCNPs and 1:5800 for core/shell UCNPs. POA copolymer (10 mg, 2.90 μmol) was stirred in 500 μL of MeOH, and 15 mL of $CHCl_3$ was added. UCNPs (0.5 nmol) in 50 μL of hexane were added, solvents evaporated under a gentle stream of N_2, and 10 mL of 10 mM MES (pH 6.0) buffer was added. The vial was sonicated for 30 min, heated at 80 °C for 45 min, cooled slowly, and sonicated again for 15 min. The UCNP dispersion was added to a 15-mL 100 kDa MWCO spin filter (Millipore), concentrated, washed 3 times with 10 mM MES (pH 6) buffer, and concentrated to a final volume of 250 μL (2 μM). Concentrations were determined using a standard emission versus concentration curve measured for the parent hydrophobic core/shell UCNPs.

2.5 UCNP-fluorophore conjugation

For functionalization of POA amines, the UCNP-fluorophore stoichiometry was varied by co-addition of MeO-PEG_8-succinimidyl ester (SE; Thermo Fisher) with the fluorophore SE, using ratios from 4:1 to 19:1 PEG:fluorophore. To fluorophore and PEG SEs (250 nmol total) in dry DMSO were added, simultaneously, 908 μL (10 pmol) of core/shell UCNPs in 10 mM MES (pH 6.0) buffer and 42 μL of 100 mM $NaHCO_3/Na_2CO_3$ (pH 11), for a final pH of just above 8. The reaction was shaken gently overnight and then purified by spin dialysis with a 500-μL 100 kDa MWCO spin filter, which was washed with 1.5 mL of 100 mM HEPES (pH 7.5) buffer, and concentrated to 150 μL (67 μM). Fluorophore:UCNP stoichiometries were determined by absorbance using known fluorophore extinction coefficients and UCNP concentrations calculated above.

2.6 Non-covalent UCNP-fluorophore coordination

Passivating UCNP oleates were removed using a protocol adapted from Bogdan.[37] Briefly, 1 mg of UCNPs in hexanes was added to a 4 mL glass vial and the hexanes evaporated under N_2. EtOH (800 μL), dH_2O (100 μL), and 0.4 M HCl (100 μL) were added to give 40 mM HCl at pH 1.4. The UCNP dispersion was sonicated for 30 min, diluted with 1 mL of dH_2O, and extracted twice against 1.5 mL of diethyl ether. Trace diethyl ether was removed from the aqueous layer under a stream of N_2 and the UCNPs washed with 12 mL of dH_2O with a 4-mL 100 kDa MWCO spin filter as above and concentrated to 110 μL. Free acids were prepared by hydrolysis of SEs (250 nmol) with 500 μL of 100 mM $NaHCO_3/Na_2CO_3$ (pH 11) in 62% (*v/v*) DMSO for 1.5 hours. HCl-treated UCNPs (0.1 nmol in 500 μL of dH_2O) and 13 μL of MeO-PEG_8-CO_2H solution (250 nmol) were added to a 500-μL 100 kDa MWCO spin filter. This solution was centrifuged through the spin filter, diluted to 500 μL, and of 250 nmol of carboxy fluorophores or PEG solution was added. The tube was purified by spin dialysis as above and concentrated to 150 μL (667 μM).

2.7 Optical characterization

Low-power upconverted emission spectra were measured from 10 nM dispersions in 10 mM HEPES, pH 7.5, with a spectrofluorometer (Horiba Jobin Yvon) equipped with a 980-nm laser (CrystaLaser) and 935/170 nm single-bandpass filter (Semrock) between laser and sample. Upconverted emission spectra were measured from 495 to 850 nm, using a 5-nm slit width and 0.1 – 1.0 s integration times. Spectra were corrected for the sensitivity of the detector using a calibrated light source. Absorbance measurements were collected on a Perkin Elmer spectrophotometer from 100 nM dispersions in 10 mM HEPES, pH 7.5. Lifetime decays were measured on an Edinburgh FLS980 instrument using a 2 ms time range and 50 Hz rep rate. Samples were diluted in D_2O. The resulting time-resolved luminescence plots were fit to exponential decays, and a weighted lifetime was calculated by

$$\tau_{eff} = \frac{\sum A_i * \tau_i}{\sum A_i}$$

where τ_{eff} is the weighted lifetime, A_i are weighting factors, τ_i are radiative lifetimes, obtained from decay curve fittings.

2.8 Electron microscopy

For TEM imaging, stock solutions of oleate-capped UCNPs were diluted 100-fold in hexane and 10 μL was adsorbed onto a carbon film/holey carbon, 400 mesh copper grid (Ted Pella). The grid was wicked of excess hexane and allowed to dry in the hood. Standard TEM images were taken with an FEI Tecnai TEM, and nanoparticle sizes were analyzed using ImageJ software by hand-drawing the diameter of each nanoparticle. Incoherent *Z*-contrast images were acquired using a high angle annular dark field detector (HAADF, Fischione) on the TEAM I aberration corrected electron microscope (Thermo Fischer Scientific) in scanning transmission (STEM) mode, with a primary beam energy of 300 keV.

2.9 Confocal imaging and spectroscopy

Images were acquired on a Zeiss 710 laser scanning confocal microscope equipped with a continuous wave 980-nm laser (Arroyo) and 34 PMTs for spectral imaging. Images were collected with a 63X 1.4NA oil objective (Plan-Apochromat DIC M27). The pixel dwell time was 177 μs and the pinhole was set to 601 μm for 980-nm imaging. The power density was calculated by measuring the laser power at the back aperture of the objective and using the area of a diffraction limited spot size. Photostability measurements were adapted from Shaner, et al. [38] [38] [38] [38] [38] [38]: briefly, mineral oil was saturated with 100 mM HEPES (pH 7.5) buffer before applying 2 μL onto a 22 × 60 mm coverslip. To the center of the 2 μL oil drop was added 1 μL of 10 nM aqueous UCNP-fluorophore conjugate or free fluorophore solution. A microscope slide was placed atop the coverslip, sealed with a spacer, and the microscope stage chamber was humidified for experiments beyond one hour. Emission acquired from Cy3-UCNPs, TAMRA-UCNPs, Cy3, and TAMRA for photostability or power series measurements were collected at 580 – 590 nm with 980 nm excitation; free cy5.5-UCNPs and cy5.5 alone were acquired at 710 – 720 nm with 561 nm excitation. Emission collected from aqueous drops, spectral reconstructions, and cell imaging with Cy3-UCNPs or pH sensor-UCNPs were collected from 500 – 700 nm taken at 3.2 – 9.7 nm PMT intervals. Images were analyzed using ImageJ. The integrated intensity of the aqueous drop was measured in a region of interest and the background was subtracted using a region of the same size containing no UCNP conjugate or fluorophore. To calculate $t_{0.5}$ values, photostability graphs were fitted to single exponential decays.

3. Results and Discussion

3.1 Synthesis and characterization of UCNPs

To engineer efficient UCNP-sensor complexes (Fig. 1a), we synthesized β-$NaYF_4$ nanocrystals doped with 20% sensitizer Yb^{3+} and a range of emitter Er^{3+} concentrations, [34] with or without 2-nm $NaYF_4$ shells[35] (Figs. 1b–e, S1, and S3). Core/shell structures were characterized by incoherent *Z*-contrast imaging with a high angle annular dark field detector (HAADF) on an aberration corrected scanning transmission electron microscope (STEM). Core/shell structures are apparent based on *Z*-contrast (Fig. S1), with an abrupt change in the intensity of the atomic columns corresponding to differences in Ln^{3+} content between core and shell, a transition not seen in the UCNP cores.

3.2 Chemical and photostability of UCNP-fluorophore conjugates

Previous work has shown that Ln^{3+} dopants in the outer 2 nm of the UCNPs are quenched by energy transfer to vibrational modes of surface ligands,[7, 11] suggesting this energy may be available to be transferred instead to proximal fluorophores (Fig. 1b, f). From hydrophobic oleate-capped UCNPs, we used two different methods to transfer UCNPs into water – acid-mediated stripping of surface oleates[37] and encapsulation within amphiphilic polymers.[36, 39] These aqueous UCNPs were then functionalized with cyanine fluorophores (Fig. S2), which are commonly used as optical sensors of reactive oxygen species (ROS).[40] For acid-treated UCNPs, fluorophore attachment occurs through the non-covalent coordination of carboxylate groups to surface cations, as has been typically used in UCNP-based sensors.[21, 24, 29] In contrast, fluorophores attach to polymer encapsulated

UCNPs by covalent conjugation of fluorophore activated esters with polymer amines (see Experimental Section).[36, 41] Polymer-encapsulated UCNP-fluorophore conjugates are free of aggregation, as shown by dynamic light scattering (DLS, Fig. S1g). Initial emission measurements of UCNP-Alexa 680 showed stronger Alexa 680 emission with coordinated fluorophores (Figs. 2a, b), but upon storage in buffer in the dark, UET dropped from 60% to 29% after 10 days (Fig. 2a). This suggests that the coordinated fluorophores are prone to dissociation from the nanocrystal when stored in buffer, consistent with previous work showing that metal ion sensors appear to dissociate from UCNPs in the presence of competitive binders (e.g., metal ions and carboxylates) inside cells.[21, 24] In contrast, polymer-encapsulated UCNPs with covalently bound Alexa 680 undergo little change over time in buffer (Fig. 2b).

Organic fluorophores are prone to degradation under the high fluences of many imaging techniques,[6, 42–45] while UCNPs do not measurably photobleach, even after exposures to single-molecule laser powers for hours.[9–10, 34] To determine how UET excitation affects fluorophore photostability under laser scanning confocal (LSC) excitation, we measured emission under continuous 980-nm excitation of core/shell UCNP-Cy3 conjugates in aqueous droplets[38] (Fig. 2c). Samples were illuminated such that emission intensities were the same at the onset of the experiment, prior to any photobleaching. The time to bleach to 50% emission intensity ($t_{0.5}$) was calculated by fitting one-phase decay curves following the >12 h exposures. Compared to direct fluorophore excitation, $t_{0.5}$ of UCNP-bound Cy3 is >100-fold longer: 83 h versus 48 min for free Cy3. Other fluorophores (TAMRA and cy5.5; see Fig. S4) also show extended longevity when excited indirectly with a 980-nm laser compared to direct excitation of the free fluorophore at visible wavelengths (Figs. S4). This unexpected improvement in longevity by UET is greater than has been achieved by strategies designed to enhance fluorophore photostability, such as attachment of triplet quenchers (up to 70-fold),[43] or less efficient methods like encapsulation within silica nanoparticles,[46] O_2 depletion, or addition of ROS scavengers.[6, 42] Enhanced fluorophore longevity by UET may be due to the low energy of NIR excitation, indirect excitation through resonant ET, or fewer encounters with collisional quenchers owing to the slower diffusion of nanoparticles. Previous work on fluorophore photobleaching has found that 2-photon excitation with NIR pulses can exacerbate photobleaching, even in large dextran-bound fluorophores,[45] and free fluorophores photobleach twice as quickly under 2-photon NIR excitation compared to standard 1-photon excitation.[47–49] In single-molecule FRET studies, both longer wavelengths and CW sources reduce photodamage,[44] suggesting the combination of these factors may be responsible for the unusual increases in observed photostability. In contrast to standard FRET experiments, in which both donor and acceptor can absorb incident photons, with UET, acceptors cannot absorb 980-nm excitation and would therefore avoid photobleaching processes such as excited-state absorption.[44, 50]

3.3 Energy transfer optimization of covalent UCNP-fluorophore conjugates

To optimize ET efficiency from UCNP to fluorophore, we analyzed the emission of UCNP-fluorophore complexes varying both fluorophore and nanoparticle structure, as well as their stoichiometry. Addition of an inert epitaxial shell leads to large enhancements in both Er^{3+}

and fluorophore emission (Fig. 3a) without a significant change in ET efficiency (Table 1). To assay the effects of stoichiometry, we included dummy PEG ligands when labeling the nanocrystals to vary the number of fluorophores per UCNP (see Experimental Section). For the hydrophilic fluorophore Cy3, whose absorbance overlaps with the green emission from the Er^{3+} $^4H_{11/2}$ and $^4S_{3/2}$ manifolds (Fig. 1b), UET is largest with 100 or fewer fluorophores per UCNP (Fig. 3b, Table 1, and Experimental Section). In contrast, the hydrophobic rhodamine TAMRA, which has a similar spectral overlap with Er^{3+}, shows lower ET efficiency (Figs. 3c and S5) and higher fluorophore:UCNP stoichiometries, possibly owing to non-covalent insertion into the hydrophobic ligand-polymer layer coating the UCNP surface (Fig. 1a). Non-specific hydrophobic association has previously been used for constructing UCNP sensors of hydrophobic analytes[23, 27] and brings the acceptor close to Er^{3+} donors, but for fluorescent acceptors we find the increased loading results in weaker UET compared to spectrally similar hydrophilic fluorophores. For these UCNP-TAMRA complexes, we observe a shortening of Er^{3+} weighted lifetimes, with the most significant changes occurring in Er^{3+} green emission bands (Figure S6 and Table S1). This is consistent with resonant energy transfer, as well as with modeling[7, 51] showing no direct pathways from the red $^4F_{9/2}$ to a green-absorbing acceptor (Figure 1b). With fewer fluorophores, Er^{3+} weighted lifetimes are similar to those of UCNPs alone, suggesting that visible Er^{3+} energy levels ($^2H_{11/2}$, $^4S_{3/2}$, $^4F_{9/2}$) may be quickly repopulated due to back-filling from Yb^{3+} or higher lying Er^{3+} manifolds (Figure S6, Table S1). In addition, recent modeling by Berry, *et al.* has shown limited emission from Er^{3+} close to the surface,[11] yet these ions are closest to surface fluorophores and therefore most likely to be resonantly coupled. This suggests a significant contribution of energy transfer from non-radiative surface Er^{3+} that may, for example, be quenched by coupling to high energy modes of oleic acid or water. The heterogeneity of Er^{3+} within the UCNP, the proximity of competing quenchers, and the presence of multiple pathways in and out of the $^2H_{11/2}$, $^4S_{3/2}$, and $^4F_{9/2}$ Er^{3+} energy levels all suggest a complexity that precludes using simple two-state lifetime equations to interpret UCNP-fluorophore ET.

For fluorophores coupled to the red-emitting Er^{3+} $^4F_{9/2}$ manifold, UET is significantly less efficient than for fluorophores coupled to the green energy levels (Figs. 3c, d and S7–8). For the hydrophobic fluorophore cy5.5, there is a significant redshift (>10 nm; Fig. 3d) in emission peak, which suggests close fluorophore-fluorophore interactions at the surface (such as J aggregates)[52] or between aggregated nanoparticles. This has been apparent in other UCNP-fluorophore spectra[29] but appears to have a significant self-quenching effect (Fig. S7) that is likely to limit the utility of these as UCNP-based sensors.

3.4 Energy transfer optimization as a function of dopant concentration and excitation power

To determine whether the presence of energy acceptors at the UCNP surface changes optimal concentrations of Ln^{3+} dopants, we evaluated UET efficiency from UCNP-fluorophore conjugates with varying Er^{3+} mole percentages at both low and high power densities. UET efficiency (Table 1) was calculated as a simple ratio of integrated emissions for a two-state system with emissive acceptor, $E = I_A/(I_A + I_D)$,[53] where the green Er^{3+} donor manifolds ($^2H_{11/2}$ and $^4S_{3/2}$) are used for I_D. Because of the complexity of the UCNP

ET pathways are not well described by a simple two-state system,[11] we also calculated ET efficiency through the loss of $^2H_{11/2}$ and $^4S_{3/2}$ emission as $E = 1 - (I_{UCNP\text{-}A}/I_{UCNP})$, where $I_{UCNP\text{-}A}$ and I_{UCNP} are the UCNP-fluorophore and UCNP emissions.[23, 54] Differences between UET efficiencies calculated using a two-state system versus donor quenching add support to lifetime measurements, that non-radiative Ln^{3+} decay pathways[7] are diverted to surface fluorophores, and this increases with elevated Er^{3+} content.

At 100 W/cm^2, Cy3 conjugates of core/shell UCNPs show increasing UET efficiency as Er^{3+} content is raised from 2 to 60% (Fig. 4a), although at the highest Er^{3+} levels overall emission is quenched. At higher power densities typical of confocal microscopy, spectral images of Cy3-conjugated UCNPs (Fig. 4b) with 20% Er^{3+} show high energy transfer at 10^5 W/cm^2 (88%; see Fig. S9 and Table 1), with a largely quenched green Er^{3+}emission. Previous work has shown that this composition (20% Yb^{3+}, 20% Er^{3+}) of unshelled UCNPs is almost non-luminescent at low powers but brighter than standard UCNPs (20% Yb^3, 2% Er^{3+}) at higher powers,[7] and suggests that, with shells, fluorophores outcompete surface oleates for Er^{3+} energy. Power series measuring Cy3 emission with either 10 or 20% Er^{3+} UCNPs (Fig. 4c) show a steep power dependence that should enable these conjugates to be used at relatively modest, 980-nm fluences. To characterize these UCNP-Cy3 conjugates in cells, they were incubated with HeLa cells and imaged for intracellular UET (Figs. 4d, e). Emission is readily apparent across a range of power densities, while Cy3 emission inside the cell under direct 516-nm excitation colocalizes to the UET signal and shows a similar punctate pattern typical of endosomal sequestration.

3.5 Mechanisms of enhanced energy transfer with UCNP-Cy3 conjugates

The increased UET for core/shell UCNPs compared to unshelled UCNPs is surprising, given that resonant ET is strongly distance-dependent, and since the shells add 2 nm between donors and acceptors. We calculated the Förster distance for 50% ET, R_0, for a single Er^{3+}-Cy3 pair (see SI Methods) using QYs of green emission ($^4H_{11/2}$, $^4S_{3/2}$) determined using a kinetic model that has been shown to calculate QYs matching experimental values (Fig. 5a).[7] At low powers, R_o is 3.2 nm using a QY of 0.8% for green Er^{3+} emission from core/shell UCNPs with 20 $Yb^{3+}$and 20% Er^{3+} (Fig. 5b), and this increases only marginally to 3.3 nm at a power density of 10^5 W/cm^2, because of the increase in QY to 1.0%. ET efficiencies would be markedly improved with higher donor QYs (SI Methods), and it is possible that heterogeneity in the Er^{3+} population within a UCNP may include ions with much higher effective QYs.[55] A homogeneous distribution of ions within the UCNP core places almost 60% of the Er^{3+} within 1 nm of the core/shell interface (Fig. 5c), or ~5–6 nm from the Cy3, based on TEM and DLS measurements of the shell and passivation layer.[36] The presence of a small number of dominant donors could account for the observed efficient ET, despite the distance between the closest Er^{3+}-Cy3 pairs.

Given the large number of fluorophores (~100) on the UCNP surface, we also examined R_n, the 50% ET distance for systems with multiple (identical) acceptors,[56–57] by

$$R_n = \left(nR_o^6\right)^{\frac{1}{6}}$$

where n is the number of acceptors. Addition of $NaYF_4$ shells to 8-nm 20% Yb^{3+}, 20% Er^{3+} UCNPs increases QY almost 300-fold,[7] which adds 3–4 nm to calculated R_n values (Fig. 5c, d) by substantially increasing R_0 (see SI Methods). This higher QY is also apparent in the 1000-fold increase in integrated visible emission of core/shell versus core Cy3-labeled UCNPs (Fig. 3a). Larger R_n values more than offset the loss in resonant ET due to the additional 2 nm between donor and acceptors, explaining how shells of just 2 nm can enhance UET efficiency in addition to overall emission. Increases in QY at higher power densities (Fig. 5a) further boost R_n, suggesting why ET at confocal laser powers is higher than for the same UCNP-fluorophore conjugates at lower powers (Fig. 3 and Table 1). These calculated R_n values suggest that multivalency is a critical component of UCNP-fluorophore conjugates, amplifying the effects of higher UCNP QY and enabling efficient UET. Simulations that account for the multiple Er^{3+} donors in addition to the multiple acceptors may lend added insight into the efficiency of UET.

4. Conclusion

We have found that the combination of thin inert shells, elevated Er^{3+} doping, multivalent acceptor labeling, and covalent conjugation to hydrophilic fluorophores enables high UET and exceptional stability for cellular imaging. While the addition of inert shells might be expected to lower UET fluorescence by adding distance between Er^{3+} and fluorophores, the large increase in UCNP QY more than compensates in both overall emission and ET efficiency, and this effect is amplified by the presence of multiple acceptors on the UCNP surface. UCNPs confer longevity on these acceptor fluorophores through indirect NIR excitation, and the photoprotective effects surpass those of fluorescent systems engineered for extreme photostability. These findings may be extended to a series of novel NIR-responsive sensors for measuring dynamic changes in pH, ion concentrations, messengers, and other chemical populations critical for cell function.

Supplementary Material

Refer to Web version on PubMed Central for supplementary material.

Acknowledgements

The authors thank Victor Mann, Angel Fernandez-Bravo, Zeming Wang, and Chris Chang for helpful discussions and comments on the manuscript. This work was supported by Cal-BRAIN award 350327 and National Institutes of Health award R01NS096317 to B.E.C. Work at the Molecular Foundry was supported by the Director, Office of Science, Office of Basic Energy Sciences, Division of Materials Sciences and Engineering, of the U.S. Department of Energy under Contract No. DE-AC02-05CH11231.

References

[1]. Aron AT; Ramos-Torres KM; Cotruvo JA; Chang CJ, Recognition- and Reactivity-Based Fluorescent Probes for Studying Transition Metal Signaling in Living Systems. Accounts of Chemical Research 2015, 48 (8), 2434–2442. [PubMed: 26215055]

[2]. Wu JS; Liu WM; Ge JC; Zhang HY; Wang PF, New sensing mechanisms for design of fluorescent chemosensors emerging in recent years. Chemical Society Reviews 2011, 40 (7), 3483–3495. [PubMed: 21445455]

[3]. Grynkiewicz G; Poenie M; Tsien RY, A new generation of Ca2+ indicators with greatly improved fluorescence properties. J Biol Chem 1985, 260 (6), 3440–50. [PubMed: 3838314]

[4]. Horton NG; Wang K; Kobat D; Clark CG; Wise FW; Schaffer CB; Xu C, In vivo three-photon microscopy of subcortical structures within an intact mouse brain. Nature Photonics 2013, 7 (3), 205–209.

[5]. Levy ES; Tajon CA; Bischof TS; Iafrati J; Fernandez-Bravo A; Garfield DJ; Chamanzar M; Maharbiz MM; Sohal VS; Schuck PJ; Cohen BE; Chan EM, Energy-Looping Nanoparticles: Harnessing Excited-State Absorption for Deep-Tissue Imaging. ACS Nano 2016, 10 (9), 8423–33. [PubMed: 27603228]

[6]. Zheng QS; Juette MF; Jockusch S; Wasserman MR; Zhou Z; Altman RB; Blanchard SC, Ultra-stable organic fluorophores for single-molecule research. Chemical Society Reviews 2014, 43 (4), 1044–1056. [PubMed: 24177677]

[7]. Gargas DJ; Chan EM; Ostrowski AD; Aloni S; Altoe MV; Barnard ES; Sanii B; Urban JJ; Milliron DJ; Cohen BE; Schuck PJ, Engineering bright sub-10-nm upconverting nanocrystals for single-molecule imaging. Nat Nanotechnol 2014, 9 (4), 300–5. [PubMed: 24633523]

[8]. Garfield DJ, B. N, Hamed SM, Torquato NA, Tajon CA, Tian B, Shevitski B, Barnard ES, Suh YD, Aloni S, Neaton JB, Chan EM, Cohen BE, Schuck PJ, Enrichment of molecular antenna triplets amplifies upconverting nanoparticle emission. Nature Photonics 2018, In press.

[9]. Nam SH; Bae YM; Park YI; Kim JH; Kim HM; Choi JS; Lee KT; Hyeon T; Suh YD, Long-Term Real-Time Tracking of Lanthanide Ion Doped Upconverting Nanoparticles in Living Cells. Angewandte Chemie-International Edition 2011, 50 (27), 6093–6097. [PubMed: 21574220]

[10]. Wu S; Han G; Milliron DJ; Aloni S; Altoe V; Talapin DV; Cohen BE; Schuck PJ, Non-blinking and photostable upconverted luminescence from single lanthanide-doped nanocrystals. Proc Natl Acad Sci U S A 2009, 106 (27), 10917–21. [PubMed: 19541601]

[11]. Hossan MY; Hor A; Luu Q; Smith SJ; May PS; Berry MT, Explaining the Nanoscale Effect in the Upconversion Dynamics of beta-NaYF4:Yb3+, Er3+ Core and Core-Shell Nanocrystals. Journal of Physical Chemistry C 2017, 121 (30), 16592–16606.

[12]. Johnson NJJ; He S; Diao S; Chan EM; Dai HJ; Almutairi A, Direct Evidence for Coupled Surface and Concentration Quenching Dynamics in Lanthanide-Doped Nanocrystals. Journal of the American Chemical Society 2017, 139 (8), 3275–3282. [PubMed: 28169535]

[13]. Wang F; Deng R; Wang J; Wang Q; Han Y; Zhu H; Chen X; Liu X, Tuning upconversion through energy migration in core-shell nanoparticles. Nat Mater 2011, 10 (12), 968–73. [PubMed: 22019945]

[14]. Jin LM; Chen X; Siu CK; Wang F; Yu SF, Enhancing Multiphoton Upconversion from NaYF4:Yb/Tm@NaYF4 Core-Shell Nanoparticles via the Use of Laser Cavity. ACS Nano 2017, 11 (1), 843–849. [PubMed: 28033468]

[15]. Rinkel T; Raj AN; Duhnen S; Haase M, Synthesis of 10 nm beta-NaYF4:Yb,Er/NaYF4 Core/Shell Upconversion Nanocrystals with 5 nm Particle Cores. Angew Chem Int Ed Engl 2016, 55 (3), 1164–7. [PubMed: 26633748]

[16]. Abel K B. J; Andrei C; van Veggel F, Analysis of the Shell Thickness Distribution on NaYF4/NaGdF4 Core/Shell Nanocrystals by EELS and EDS. J. Phys. Chem. Lett 2011, 2 (3), 185–189.

[17]. Kilbane JD; Chan EM; Monachon C; Borys NJ; Levy ES; Pickel AD; Urban JJ; Schuck PJ; Dames C, Far-field optical nanothermometry using individual sub-50 nm upconverting nanoparticles. Nanoscale 2016, 8 (22), 11611–6. [PubMed: 27216164]

[18]. Sedlmeier A; Achatz DE; Fischer LH; Gorris HH; Wolfbeis OS, Photon upconverting nanoparticles for luminescent sensing of temperature. Nanoscale 2012, 4 (22), 7090–6. [PubMed: 23070055]

[19]. Lay A; Wang DS; Wisser MD; Mehlenbacher RD; Lin Y; Goodman MB; Mao WL; Dionne JA, Upconverting Nanoparticles as Optical Sensors of Nano- to Micro-Newton Forces. Nano Letters 2017, 17 (7), 4172–4177. [PubMed: 28608687]

[20]. Esipova TV; Ye X; Collins JE; Sakadzic S; Mandeville ET; Murray CB; Vinogradov SA, Dendritic upconverting nanoparticles enable in vivo multiphoton microscopy with low-power continuous wave sources. Proc Natl Acad Sci U S A 2012, 109 (51), 20826–31. [PubMed: 23213211]

[21]. Li Z; Lv S; Wang Y; Chen S; Liu Z, Construction of LRET-based nanoprobe using upconversion nanoparticles with confined emitters and bared surface as luminophore. J Am Chem Soc 2015, 137 (9), 3421–7. [PubMed: 25707940]

[22]. Liu Q; Peng J; Sun L; Li F, High-efficiency upconversion luminescent sensing and bioimaging of Hg(II) by chromophoric ruthenium complex-assembled nanophosphors. ACS Nano 2011, 5 (10), 8040–8. [PubMed: 21899309]

[23]. Liu Y; Chen M; Cao T; Sun Y; Li C; Liu Q; Yang T; Yao L; Feng W; Li F, A cyanine-modified nanosystem for in vivo upconversion luminescence bioimaging of methylmercury. J Am Chem Soc 2013, 135 (26), 9869–76. [PubMed: 23763640]

[24]. Peng J; Xu W; Teoh CL; Han S; Kim B; Samanta A; Er JC; Wang L; Yuan L; Liu X; Chang YT, High-efficiency in vitro and in vivo detection of Zn2+ by dye-assembled upconversion nanoparticles. J Am Chem Soc 2015, 137 (6), 2336–42. [PubMed: 25626163]

[25]. Zhou L; Wang R; Yao C; Li XM; Wang CL; Zhang XY; Xu CJ; Zeng AJ; Zhao DY; Zhang F, Single-band upconversion nanoprobes for multiplexed simultaneous in situ molecular mapping of cancer biomarkers. Nature Communications 2015, 6.

[26]. Arppe R; Nareoja T; Nylund S; Mattsson L; Koho S; Rosenholm JM; Soukka T; Schaferling M, Photon upconversion sensitized nanoprobes for sensing and imaging of pH. Nanoscale 2014, 6 (12), 6837–43. [PubMed: 24827972]

[27]. Cheng L Y. K; Shao M; SLee S-T; Liu Z, Multicolor In Vivo Imaging of Upconversion Nanoparticles with Emissions Tuned by Luminescence Resonance Energy Transfer. J. Phys. Chem. C 2011, 115, 2686–2692.

[28]. Dukhno O; Przybilla F; Collot M; Klymchenko A; Pivovarenko V; Buchner M; Muhr V; Hirsch T; Mely Y, Quantitative assessment of energy transfer in upconverting nanoparticles grafted with organic dyes. Nanoscale 2017, 9 (33), 11994–12004. [PubMed: 28795714]

[29]. Muhr V; Wurth C; Kraft M; Buchner M; Baeumner AJ; Resch-Genger U; Hirsch T, Particle-Size-Dependent Forster Resonance Energy Transfer from Upconversion Nanoparticles to Organic Dyes. Anal Chem 2017, 89 (9), 4868–4874. [PubMed: 28325045]

[30]. Zhang P; Rogelj S; Nguyen K; Wheeler D, Design of a highly sensitive and specific nucleotide sensor based on photon upconverting particles. J Am Chem Soc 2006, 128 (38), 12410–1. [PubMed: 16984179]

[31]. Drees C; Raj AN; Kurre R; Busch KB; Haase M; Piehler J, Engineered Upconversion Nanoparticles for Resolving Protein Interactions inside Living Cells. Angew Chem Int Ed Engl 2016, 55 (38), 11668–72. [PubMed: 27510808]

[32]. Li C; Zuo J; Zhang L; Chang Y; Zhang Y; Tu L; Liu X; Xue B; Li Q; Zhao H; Zhang H; Kong X, Accurate Quantitative Sensing of Intracellular pH based on Self-ratiometric Upconversion Luminescent Nanoprobe. Sci Rep 2016, 6, 38617. [PubMed: 27934889]

[33]. Wang Y, L. K, Liu X, Dohnalová K, Gregorkiewicz T, Kong X, Aalders M, Buma W, Zhang H, Critical Shell Thickness of Core/Shell Upconversion Luminescence Nanoplatform for FRET Application. J. Phys. Chem. Lett 2011, 2 (17), 2083–2088.

[34]. Ostrowski AD; Chan EM; Gargas DJ; Katz EM; Han G; Schuck PJ; Milliron DJ; Cohen BE, Controlled synthesis and single-particle imaging of bright, sub-10 nm lanthanide-doped upconverting nanocrystals. ACS Nano 2012, 6 (3), 2686–92. [PubMed: 22339653]

[35]. Li XM; Shen DK; Yang JP; Yao C; Che RC; Zhang F; Zhao DY, Successive Layer-by-Layer Strategy for Multi-Shell Epitaxial Growth: Shell Thickness and Doping Position Dependence in Upconverting Optical Properties. Chemistry of Materials 2013, 25 (1), 106–112.

[36]. Wichner SM; Mann VR; Powers AS; Segal MA; Mir M; Bandaria JN; DeWitt MA; Darzacq X; Yildiz A; Cohen BE, Covalent Protein Labeling and Improved Single-Molecule Optical Properties of Aqueous CdSe/CdS Quantum Dots. ACS Nano 2017, 11 (7), 6773–6781. [PubMed: 28618223]

[37]. Bogdan N; Vetrone F; Ozin GA; Capobianco JA, Synthesis of ligand-free colloidally stable water dispersible brightly luminescent lanthanide-doped upconverting nanoparticles. Nano Lett 2011, 11 (2), 835–40. [PubMed: 21244089]

[38]. Shaner NC C. RE; Steinbach PA; Giepmans BNG; Palmer AE; Tsien RT, Improved monomeric red, orange and yellow fluorescent proteins derived from Discosoma sp. red fluorescent protein. Nature Biotechnology 2004, 22, 1567–1572.

[39]. Pellegrino T; Manna L; Kudera S; Liedl T; Koktysh D; Rogach AL; Keller S; Radler J; Natile G; Parak WJ, Hydrophobic nanocrystals coated with an amphiphilic polymer shell: A general route to water soluble nanocrystals. Nano Letters 2004, 4 (4), 703–707.

[40]. Kundu K; Knight SF; Willett N; Lee S; Taylor WR; Murthy N, Hydrocyanines: a class of fluorescent sensors that can image reactive oxygen species in cell culture, tissue, and in vivo. Angew Chem Int Ed Engl 2009, 48 (2), 299–303. [PubMed: 19065548]

[41]. Albers AE; Chan EM; McBride PM; Ajo-Franklin CM; Cohen BE; Helms BA, Dual-emitting quantum dot/quantum rod-based nanothermometers with enhanced response and sensitivity in live cells. J Am Chem Soc 2012, 134 (23), 9565–8. [PubMed: 22642769]

[42]. Aitken CE; Marshall RA; Puglisi JD, An oxygen scavenging system for improvement of dye stability in single-molecule fluorescence experiments. Biophysical Journal 2008, 94 (5), 1826–1835. [PubMed: 17921203]

[43]. Altman RB; Zheng Q; Zhou Z; Terry DS; Warren JD; Blanchard SC, Enhanced photostability of cyanine fluorophores across the visible spectrum. Nat Methods 2012, 9 (5), 428–9. [PubMed: 22543373]

[44]. Kong XX; Nir E; Hamadani K; Weiss S, Photobleaching pathways in single-molecule FRET experiments. Journal of the American Chemical Society 2007, 129 (15), 4643–4654. [PubMed: 17375921]

[45]. Patterson GH; Piston DW, Photobleaching in two-photon excitation microscopy. Biophysical Journal 2000, 78 (4), 2159–2162. [PubMed: 10733993]

[46]. Ow H; Larson DR; Srivastava M; Baird BA; Webb WW; Wiesner U, Bright and stable core-shell fluorescent silica nanoparticles. Nano Letters 2005, 5 (1), 113–117. [PubMed: 15792423]

[47]. Sanchez EJ, N. L, Holtom GR, Xie XS, Room-Temperature Fluorescence Imaging and Spectroscopy of Single Molecules by Two-Photon Excitation. J. Phys. Chem. A 1997, 101 (38), 7019–7023.

[48]. Schuck PJ WK, Fromm DP, Twieg RJ, Moerner WE, A novel fluorophore for two-photon-excited single-molecule fluorescence. Chemical Physics 2005, 318, 7–11.

[49]. Willets KA; Ostroverkhova O; He M; Twieg RJ; Moerner WE, Novel fluorophores for single-molecule imaging. J Am Chem Soc 2003, 125 (5), 1174–5. [PubMed: 12553812]

[50]. Eggeling C; Widengren J; Brand L; Schaffer J; Felekyan S; Seidel CA, Analysis of photobleaching in single-molecule multicolor excitation and Forster resonance energy transfer measurements. J Phys Chem A 2006, 110 (9), 2979–95. [PubMed: 16509620]

[51]. Chan EM; Han G; Goldberg JD; Gargas DJ; Ostrowski AD; Schuck PJ; Cohen BE; Milliron DJ, Combinatorial Discovery of Lanthanide-Doped Nanocrystals with Spectrally Pure Upconverted Emission. Nano Letters 2012, 12 (7), 3839–3845. [PubMed: 22713101]

[52]. Wurthner F; Kaiser TE; Saha-Moller CR, J-Aggregates: From Serendipitous Discovery to Supramolecular Engineering of Functional Dye Materials. Angewandte Chemie-International Edition 2011, 50 (15), 3376–3410. [PubMed: 21442690]

[53]. Osad'ko IS, Dependence of FRET efficiency on distance in single donor-acceptor pairs. J Chem Phys 2015, 142 (12), 125102. [PubMed: 25833609]

[54]. Lakowicz JR, Principles of Fluorscence Spectroscopy. 3 ed.; Springer US: 2006.

[55]. Li X; Wang R; Zhang F; Zhao D, Engineering homogeneous doping in single nanoparticle to enhance upconversion efficiency. Nano Lett 2014, 14 (6), 3634–9. [PubMed: 24874018]

[56]. Corry B; Jayatilaka D; Rigby P, A flexible approach to the calculation of resonance energy transfer efficiency between multiple donors and acceptors in complex geometries. Biophys J 2005, 89 (6), 3822–36. [PubMed: 16199497]

[57]. Fabian AI; Rente T; Szollosi J; Matyus L; Jenei A, Strength in numbers: effects of acceptor abundance on FRET efficiency. Chemphyschem 2010, 11 (17), 3713–21. [PubMed: 20936620]

[58]. Boyer JC; van Veggel FC, Absolute quantum yield measurements of colloidal NaYF4: Er3+, Yb3+ upconverting nanoparticles. Nanoscale 2010, 2 (8), 1417–9. [PubMed: 20820726]

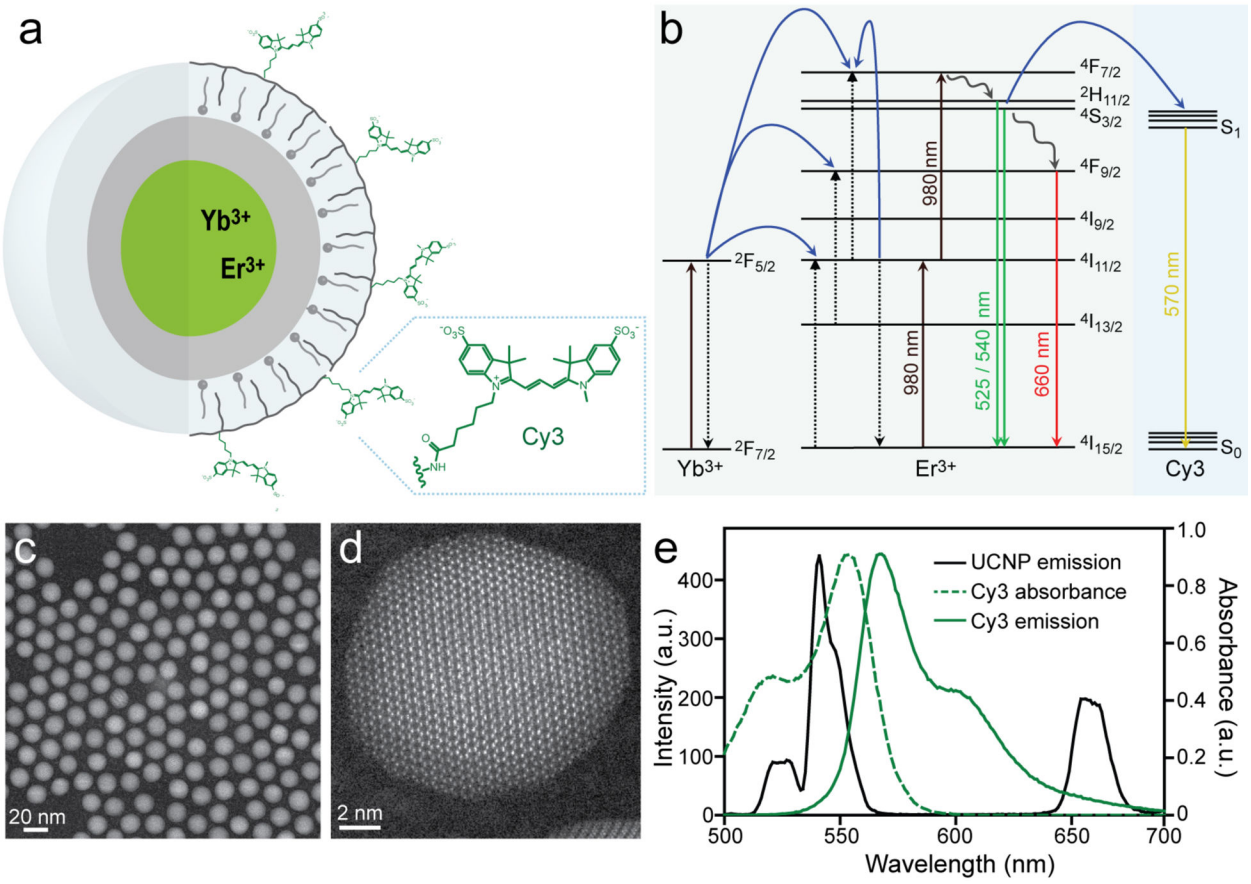

Fig. 1.

Design of UCNP-fluorophore conjugates for efficient upconverted energy transfer. (a) Yb^{3+}, Er^{3+}-doped core/shell UCNPs encapsulated in fluorophore-conjugated amphiphilic polymers. (b) Energy diagram for energy transfer from UCNPs complexed with fluorophore Cy3. UCNP energy pathways calculated as in ref [7]. (c) *Z*-contrast STEM image of 8-nm β-$NaYF_4$: 20% Yb, 20% Er UCNPs with 2-nm $NaYF_4$ shells. Scale bar is 20 nm. (d) Incoherent *Z*-contrast STEM image of 10-nm $NaErF_4$ UCNPs with 2-nm $NaYF_4$ shell. Scale bar is 6 nm. (e) Absorbance and emission spectra of Cy3 overlaid with visible UCNP emission spectrum from 980 nm excitation.

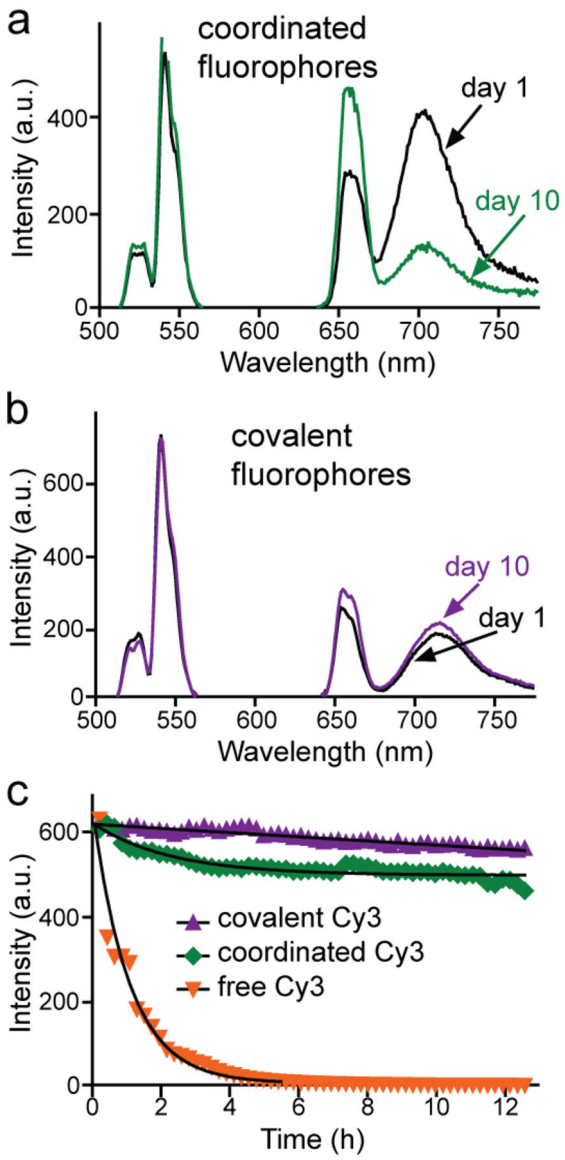

Fig. 2.

Chemical and photostability of UCNP-fluorophore complexes. Change in UET emission of fluorophores after 10 days *without* light exposure of Alexa 680 either (a) coordinated directly to the UCNP surface, or (b) covalently attached to passivating UCNP polymer. (c) UET emission of UCNP-bound Cy3 under sustained excitation of 10^5 W/cm^2 980 nm CW laser, either covalently attached or coordinated to the surface. Images were acquired from aqueous droplets every 13 mins for >12 hrs. Free Cy3 was directly excited at 514 nm to give comparable initial signal as UCNP-Cy3 complexes excited at 980 nm. Times to photobleach to 50% emission are: 83 h, 51 h, and 0.80 h for covalently attached, coordinated, or free Cy3, respectively. Core/shell UCNPs used in these experiments are 8-nm β-$NaYF_4$: 20% Yb, 20% Er with 2-nm $NaYF_4$ shells.

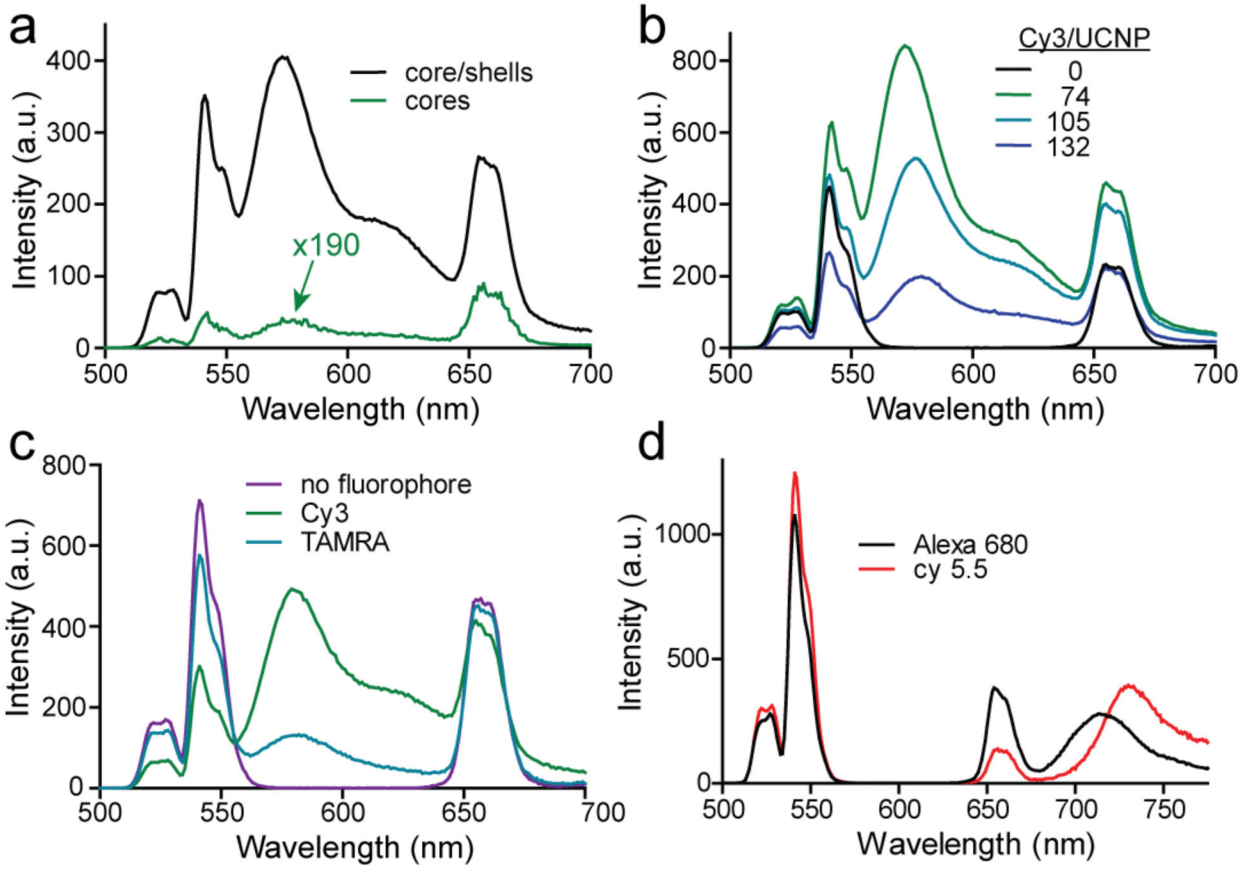

Fig. 3.

Optimizing energy transfer in covalent UCNP-fluorophore complexes. (a) Upconverted emission spectra of 8-nm 20% Yb, 20% Er-doped UCNPs with or without (shown magnified 190x) 2-nm $NaYF_4$ shells. Upconverted emission spectra of core/shell UCNPs varying (b) fluorophore:UCNP stoichiometry; fluorophores coupled to (c) Er^{3+} green emission (Cy3, TAMRA), or (d) Er^{3+} red emission (Alexa 680, cy5.5). All spectra are normalized to UCNP-fluorophore concentration, as described in Methods.

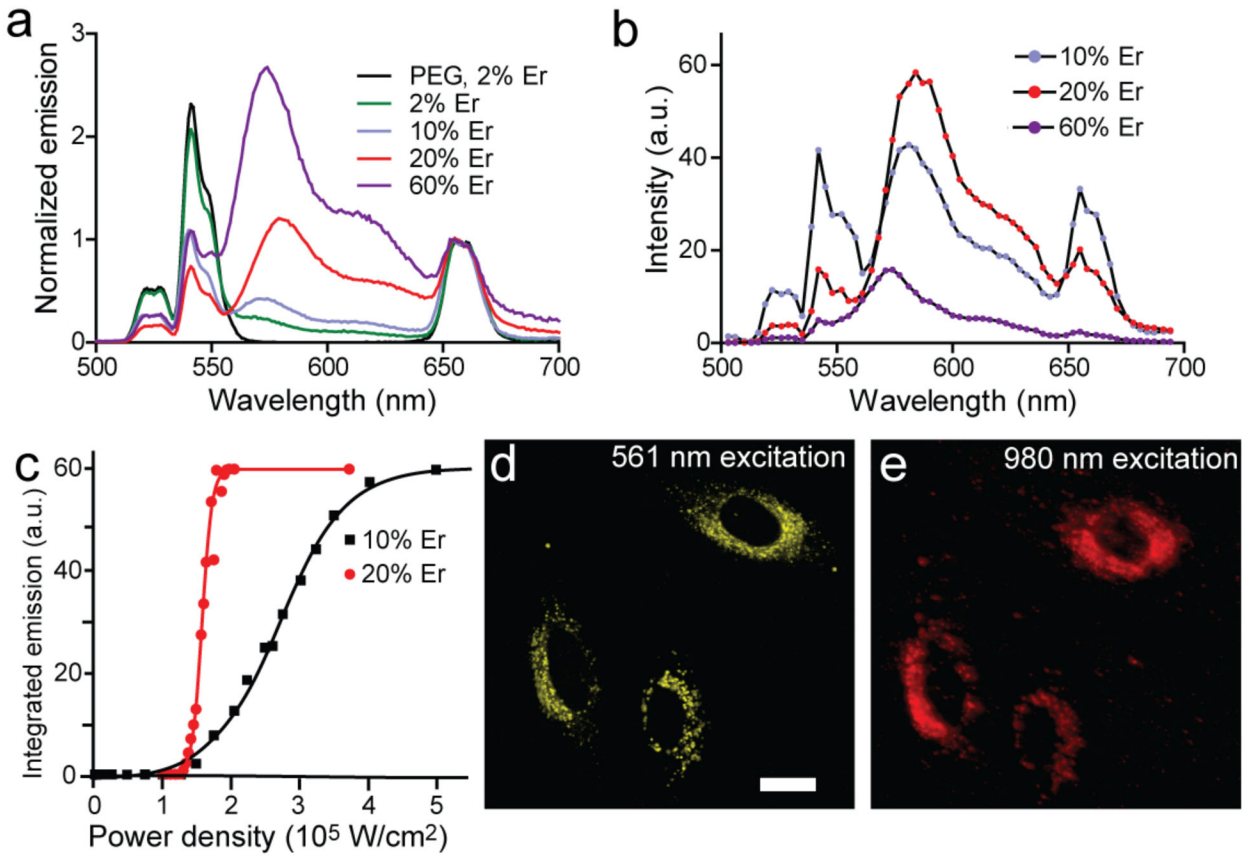

Fig. 4.

Optimization of upconverted energy transfer as a function of excitation density. (a) Upconverted emission spectra of covalent core/shell UCNP-fluorophore conjugates bearing ~100 Cy3 per UCNP as a function of Er^{3+} content at low 980 nm excitation density (100 W/cm^2). Spectra are normalized to 655 nm emission. (b) Confocal spectral imaging of covalent core/shell UCNP-Cy3 conjugates as a function of Er^{3+} content at higher fluences (10^5 W/cm^2 for 20% Er^{3+} and 10^6 W/cm^2 for the others). (c) Power dependence of Cy3 emission for conjugates in (b) with 10% or 20% Er^{3+}. Integrated emission is 560 – 640 nm, and its maximum is due to detector saturation. (d, e) Confocal images of HeLa cells with endocytosed covalent UCNP-Cy3 conjugates excited at either 561 nm or 980 nm. UCNPs are β-$NaYF_4$: 20% Yb, 20% Er @ $NaYF_4$. Scale bar is 20 μm.

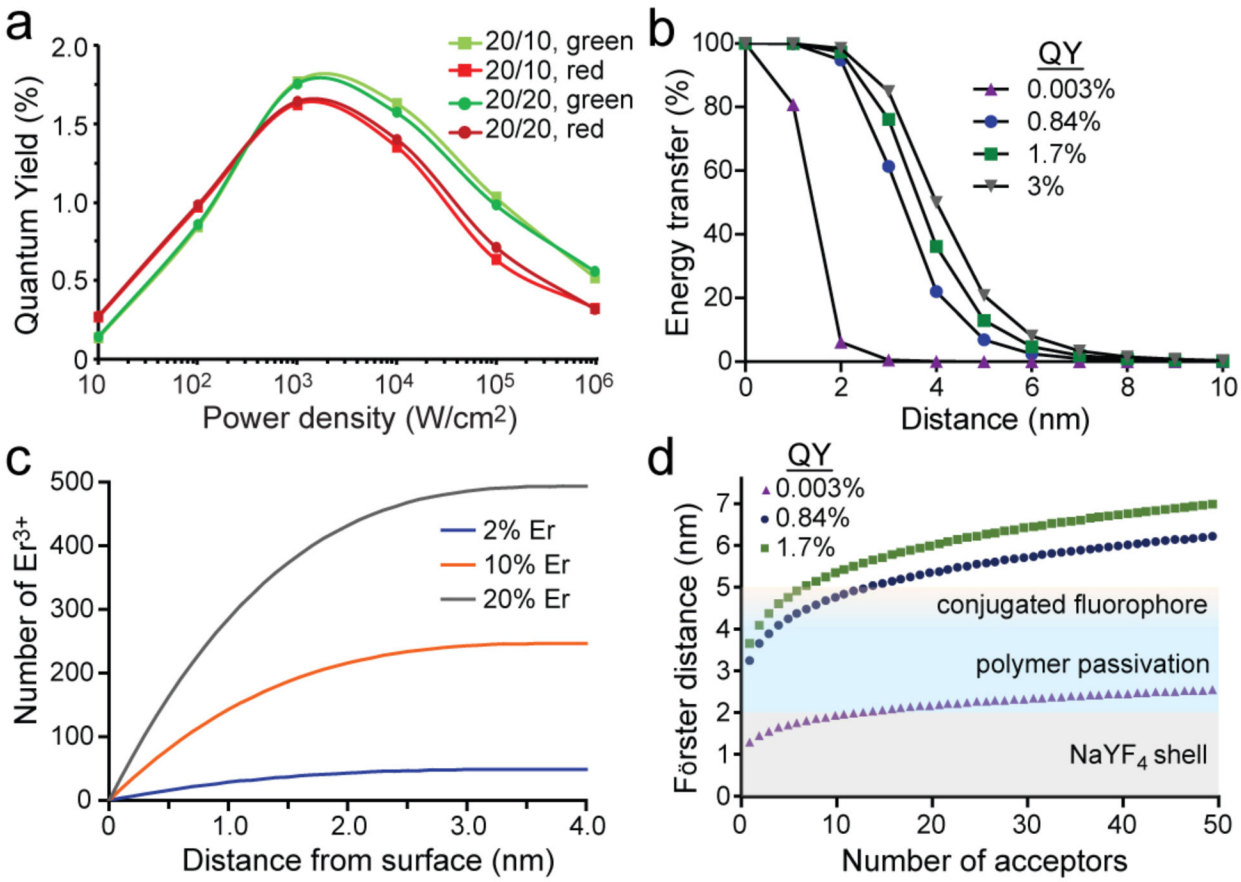

Fig. 5.

Mechanisms of observed UET with UCNP-Cy3 donor/acceptors. (a) Quantum yields of core/shell UCNP green and red manifolds as a function of power density, calculated with kinetic simulations of Yb^{3+}, Er^{3+} pathways.[7, 51] (b) Calculated ET efficiencies for single Er^{3+}-single Cy3 donor/acceptor pairs, varying the quantum yield of the donor, based on the Förster equation. QY values are calculated and experimental values for unshelled 8-nm $NaYF_4$: 20% Yb, 20% Er (QY = 0.003%),[7] and shelled 8-nm $NaYF_4$: 20% Yb, 20% Er at low (QY = 0.84%)[7] and high (QY = 1.7%) power densities as in (a). For bulk upconverting materials with Yb and Er, QY = 3%.[58] (c) Calculated distance from surface of Er^{3+} ions in an 8-nm UCNP, assuming a homogeneous distribution of dopants. (d) Calculated multi-acceptor Er^{3+}-Cy3 Förster distances, R_n, as a function of donor QY and number of acceptors.[57] QY values are as in (b). Colors represent TEM and DLS-measured distances[36] from core surface to epitaxial shell (gray), organic passivation (blue), and Cy3 (yellow).

Table 1.

Measured UET efficiencies of UCNP-fluorophore conjugates. Number of fluorophores per UCNP are calculated as in Experimental Section.

Er^{3+} content (%)	shell radius (nm)	Fluorophores:UCNP	Power density (W/cm^2)	Attachment	2-state ET (%)	Loss of donor ET (%)
2	2	105 Cy3	10^2	covalent	24	6
10	2	105 Cy3	10^2	covalent	52	16
10	2	105 Cy3	10^6	covalent	71	45
20	0	74 Cy3	10^2	covalent	72	-
20	2	74 Cy3	10^2	covalent	76	-
20	2	105 Cy3	10^2	covalent	79	49
20	2	105 Cy3	10^5	covalent	88	61
20	2	105 Alexa 680	10^2	covalent	29	-
20	2	315 Alexa 680	10^2	coordinated	60	-
20	2	400 cy5.5	10^2	covalent	44	-
20	2	400 TAMRA	10^2	covalent	40	-
60	2	105 Cy3	10^2	covalent	85	20
60	2	105 Cy3	10^6	covalent	83	23

*hydrophobic TAMRA and cy5.5 fluorophores are also likely bound through non-specific interactions with the passivating oleate/polymer layer